International Journal of Applied Earth Observation and Geoinformation 123 (2023) 103470

Contents lists available at ScienceDirect

International Journal of Applied Earth Observation and Geoinformation

journal homepage: www.elsevier.com/locate/jag

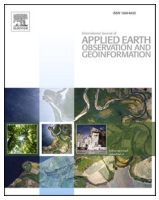

Optimal spectral index and threshold applied to Sentinel-2 data for extracting impervious surface: Verification across latitudes, growing seasons, approaches, and comparison to global datasets

Yury Dvornikov [a,b,*], Valentina Grigorieva [a], Mikhail Varentsov [c,d,e], Viacheslav Vasenev [f]

[a] Smart Urban Nature Laboratory, RUDN University, 117198 Moscow, Miklukho-Maklaya str., 8/2, Russian Federation
[b] Laboratory of Carbon Monitoring in Terrestrial Ecosystems, Institute of Physicochemical and Biological Problems of Soil Science of the Russian Academy of Sciences, 142290 Pushchino, Institutskaya str., 2, Russian Federation
[c] Research Computing Center / Faculty of Geography, Lomonosov Moscow State University, 119991 Moscow, GSP-1, Leninskie Gory str., 1-12, Russian Federation
[d] A.M. Obukhov Institute of Atmospheric Physics, 119017 Moscow, Pyzhevskii Lane, 3, Russian Federation
[e] Hydrometeorological Research Centre of Russian Federation, 123376 Moscow, Bolshoy Predtechensky Lane, 13/1, Russian Federation
[f] Soil Geography and Landscape Group, Wageningen University, 6700AA Wageningen, Netherlands

ARTICLE INFO

Keywords:
Imperviousness
Urban environment
Latitudinal transect
Spectral unmixing
Spectral transformation
Global datasets

ABSTRACT

Many spectral indices have recently been developed for accurate extraction of impervious surfaces. Moreover, there are several 10-m global datasets available containing urban/impervious land cover class claiming to be of high accuracy. Up to date, there was no detailed analysis on the influence of easy-to-calculate spectral index and threshold on the final accuracy at large scale applied to Sentinel-2 scenes. Furthermore, the impact of growing season and the land-use type is unclear and the available global datasets must be validated in terms of their applicability for the accurate extraction of impervious surface for urban ecological applications. We show that the highest accuracy can be obtained by applying mNDVI and UCI thresholds (0.41 and −0.49 respectively) for summer median composites of Sentinel-2A/B acquisitions (highest R^2>0.82 and lowest RMSE<10%) if validated against true imperviousness on the areal basis. In cases, where the number of cloud-free scenes is insufficient, an established growing season shall be used. Small artificial patches possess the highest uncertainty at this resolution, but not exceeding 20%. Spectral unmixing applied to pixels extracted using the thresholds do not significantly improve the overall estimates. Only ESA Worldcover 10-m demonstrated the comparable R^2 and RMSE metrics among global datasets. Moreover, compared global datasets showed significant differences (up to tens of %) between the impervious surface estimates for selected ten cities, that highlights further evaluations of these data. Our results can successfully be implemented for mapping annual and even seasonal dynamics of imperviousness within the urban environment.

1. Introduction

Ongoing urbanization coincides with remarkable environmental consequences, among which soil sealing has likely the highest negative impact on urban ecosystems (Kabisch and Haase, 2013; Xiao et al., 2013). Sealed soils or impervious surfaces can be defined as the proportion of any material that prevents the infiltration of water into the soil (Arnold and Gibbons, 1996). Soil sealing occurring on former arable lands is considered by European Union among the principle threats for soil fertility and health (Ceccarelli et al., 2014; European Commission, 2012; EEA, 2010). Soil sealing depletes the most valuable soil functions including carbon sequestration (Romzaykina et al., 2020), microbial diversity and activity (Piotrowska-Długosz and Charzyński, 2015), and soil buffer capacity as geochemical barriers for pollutants (Romzaykina et al., 2021). Indirectly, soil sealing affects urban climate and air quality by being one of the key factors in the emergence of a urban heat island (Varentsov et al., 2020). Due to the effect of soil sealing on the local climate, surface imperviousness becomes a key input parameter for meteorological models when they are applied for weather and climate forecasts in urban areas (Apreda et al., 2023; Masson et al., 2020). Therefore, an accurate quantitative assessment of soil sealing dynamics at the city-level is needed to support spatial planning and sustainable

* Corresponding author at: Smart Urban Nature Laboratory, RUDN University, 117198 Moscow, Miklukho-Maklaya str., 8/2, Russian Federation.
E-mail address: dvornikov_yua@pfur.ru (Y. Dvornikov).

https://doi.org/10.1016/j.jag.2023.103470
Received 11 June 2023; Received in revised form 27 July 2023; Accepted 22 August 2023
Available online 31 August 2023

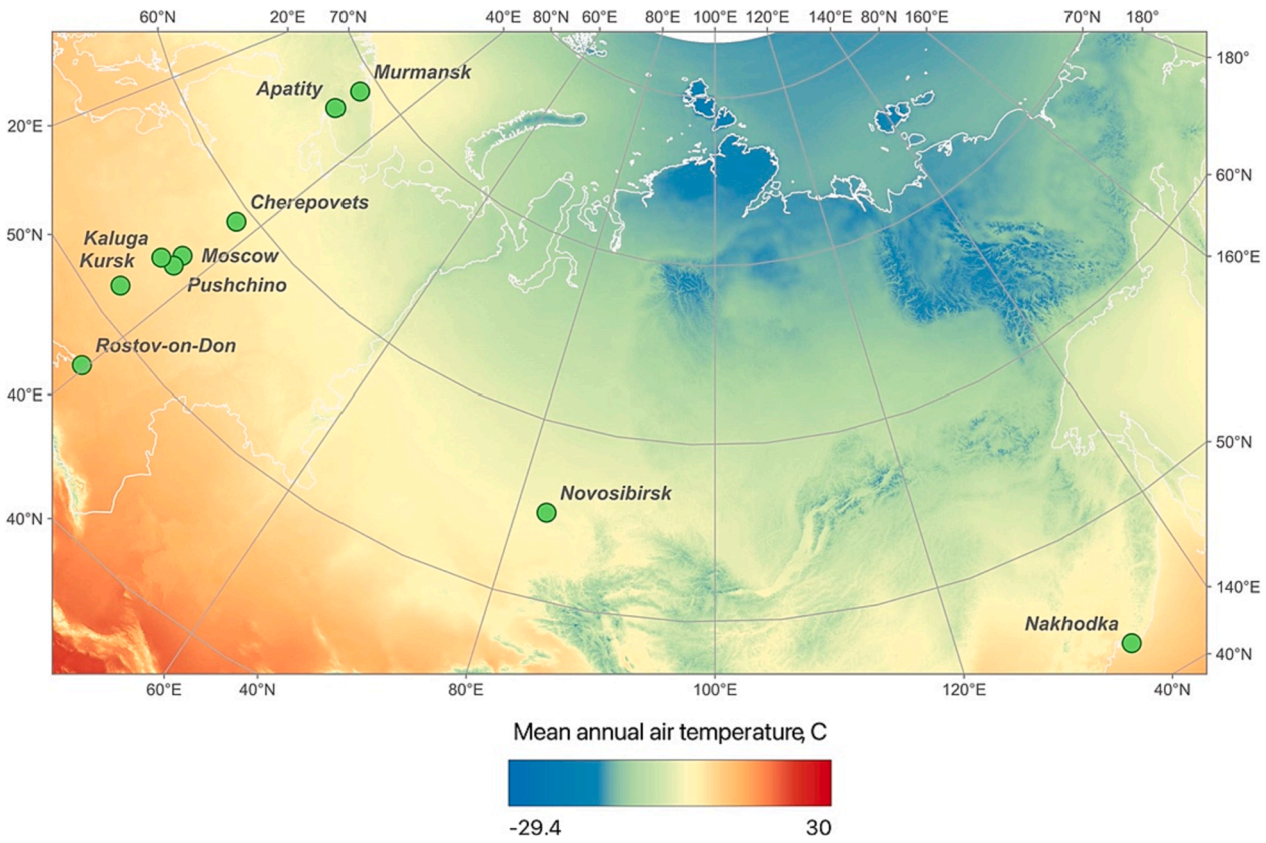

Fig. 1. Location of test cities. Background dataset – CHELSA mean annual air temperature (Karger et al., 2017).

Table 1
Characteristics of selected cities (from the north to south).

City	Established in	Area, km^2	Climate (updated Köppen-Geiger classes) (Beck et al., 2018)	Population (2021)	Main economic activity
Murmansk	1916	154.4	Dfc Cold, no dry season, cold summer	270,384	Transport (marine port)
Apatity	1926	37.5	Dfc Cold, no dry season, cold summer	49,647	Industry (mining)
Cherepovets	1777	131	Dfb Cold, no dry season, warm summer	309,445	Industry (ferrous metallurgy, chemistry)
Moscow	1147	2561.5	Dfb Cold, no dry season, warm summer	13,010,112	Megapolis
Novosibirsk	1893	502.7	Dfb Cold, no dry season, warm summer	1,633,595	Science, industry (high-tech)
Pushchino	1956	18.23	Dfb Cold, no dry season, warm summer	19,578	Science
Kaluga	1371	168.8	Dfb Cold, no dry season, warm summer	337,058	Historical, culture
Kursk	1095	208.2	Dfb Cold, no dry season, warm summer	440,052	Agriculture, electrical industry
Rostov-on-Don	1749	348.5	Dfa Cold, no dry season, hot summer	1,142,162	Transport (river port), agriculture
Nakhodka	1864	325.9	Dwb Cold, dry winter, warm summer	139,931	Transport (marine port)

development of urban areas, which is clearly reflected in requests from architects and urban planners.

The first attempts to apply algorithms aiming at extracting impervious area percentage were made right after the launch of ERTS (Landsat-1) satellite in 1972 by applying an empirical relationship between the surface reflectance of the Landsat ground resolved area and the known percent of the impervious area (Jackson, 1975; Jackson and McCuen, 1979). In the end of 20th century, many researches have already been conducted aiming to find an accurate method for assessment of imperviousness by utilising a new MSS (Jackson and McCuen, 1979), TM (Plunk et al., 1990) and HRV (Ehlers et al., 1990; Gong and Howarth, 1990; Morgan et al., 1993) sensors at 10/20/30/79m of ground resolved distances (Slonecker et al., 2001 and references therein). Based on the traditional LULC classification units (Anderson et al., 1976), authors considered transportation infrastructure, rooftops, sidewalks, parking lots and other human-made infrastructure as the class “impervious area”. Over the last decades, a considerable progress was achieved in mapping impervious surface (Weng, 2012). This progress was possible due to substantial improvements in data quality of the satellite images (i.e. spatial, radiometric and spectral resolution) and significantly developed pixel-, subpixel- and object-based classification algorithms. The data from recently launched Sentinel-2A/B satellites have been successfully tested for mapping urban land-use zoning and land cover categories (Xian et al., 2019; Xu et al., 2018). Per-pixel and sub-pixel algorithms have shown a robust (>80% accuracy) results in extracting such categories as impervious surface, bare soils and vegetation within the urban landscape (Dvornikov et al., 2021; Xu et al., 2018). Studies show that the optimal spatial resolution of the initial data is within the range of 5–20 m (Welch, 1982; Xian et al., 2019), since more detailed data can introduce significant errors in the estimates of imperviousness and other land-cover classes. Global experience in the analysis of imperviousness in cities has included the use of threshold-based segmentation using various easy-to-apply spectral transformation indices as input data, such as the normalized difference vegetation index (NDVI) (Tucker, 1979), the normalized difference built-up index (NDBI) (Zha et al., 2003), the values of the transformed

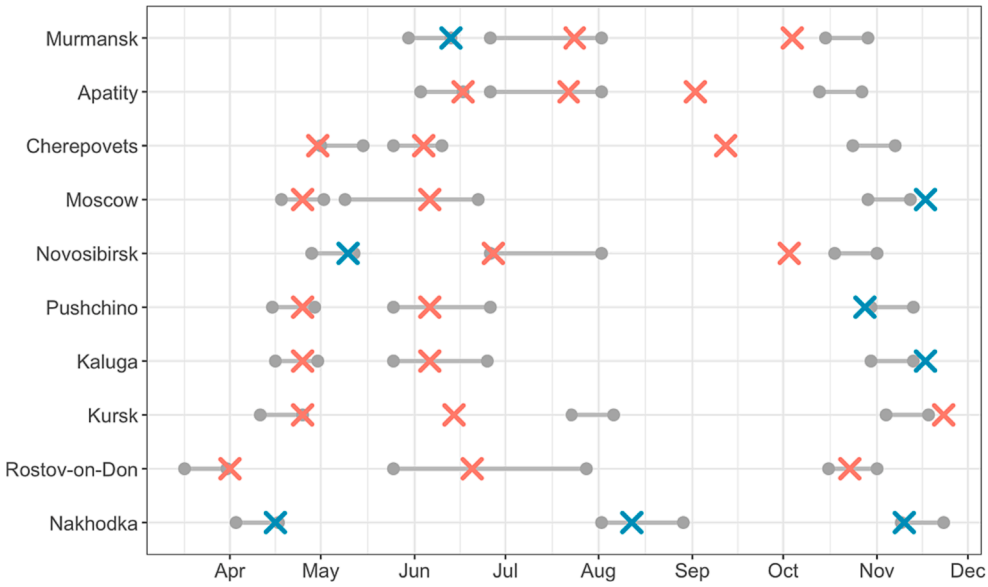

Fig. 2. Duration of identified periods of growing seasons: onset, middle, and the end (gray lines) with corresponding acquisition dates of Sentinel-2A/B (red crosses – 2019, blue – 2020).

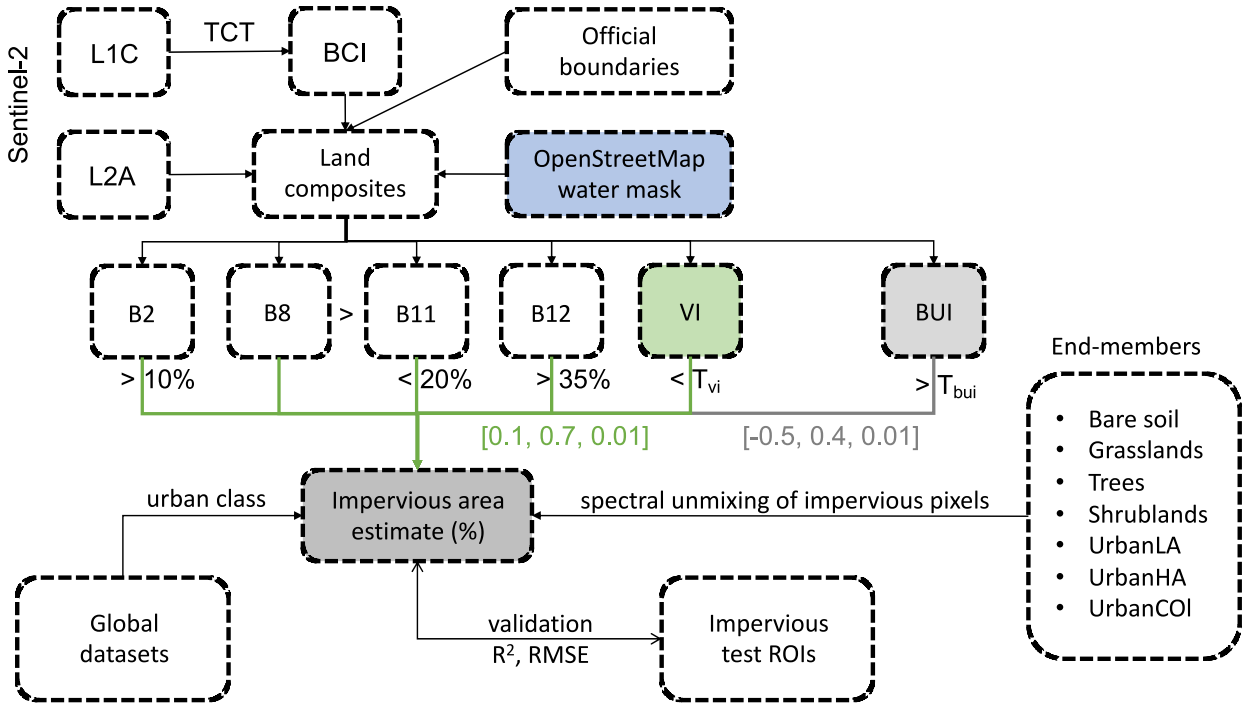

Fig. 3. Analysis workflow: L1C – Top of Atmosphere reflectance; L2A – surface reflectance; official boundaries – vector data according to Rosreestr©; OpenStreetMap water mask – vector water mask extracted from OSM data; TCT – Tasseled Cap Transformation; BCI – a biophysical component index after (Deng and Wu, 2012); B2, B8, B11, B12 – surface reflectance in the blue, near-infrared, shortwave infrared 1 (1614/1610 nm), and shortwave infrared 2 (2202/2186 nm) correspondingly; VI – vegetation indices (mNDVI and mSAVI), T_{vi} – threshold for VI (from 0.1 to 0.7 with 0.01 step); BUI – a bunch of built-up spectral indices described in 2.2.2; T_{vi} - threshold for BUI (from −0.5 to 0.4 with 0.01 step); UrbanLA – urban low albedo spectral signature; UrbanHA – urban high albedo spectral signature; UrbanCOL – urban colored roofs spectral signature; global datasets – four global 10-m estimates of the impervious / built-up land cover class as described above.

images (for example, Tasselled Cap, as well as the bio-physical composition index (BCI) (Deng and Wu, 2012), and other spectral indices (Feng and Fan, 2021; Tian et al., 2018; Xu, 2008). Methods such as decision trees, convolutional neural networks, spectral mixture analysis, and regression have been used as classification methods (Li, 2020 and references therein). Recently, a wide range of novel machine learning algorithms have been applied to multi-source data such as optical and synthetic aperture radar (SAR) remote sensing data for mapping and projecting imperviousness (Parekh et al., 2021; Zhang et al., 2014). Normally, developed algorithms are tested over one to three cities. We hypotesize that the accuracy of impervious surface extraction using the certain method would in fact depend on the geographic location, growing season, and is a subject of a mapped land-use type. In this paper we have reviewed the accuracy of impervious surface extraction from Sentinel-2 data as a function of 1) spectral transformation method; 2) its threshold, 3) geographic settings; 4) major econimic activity type of the

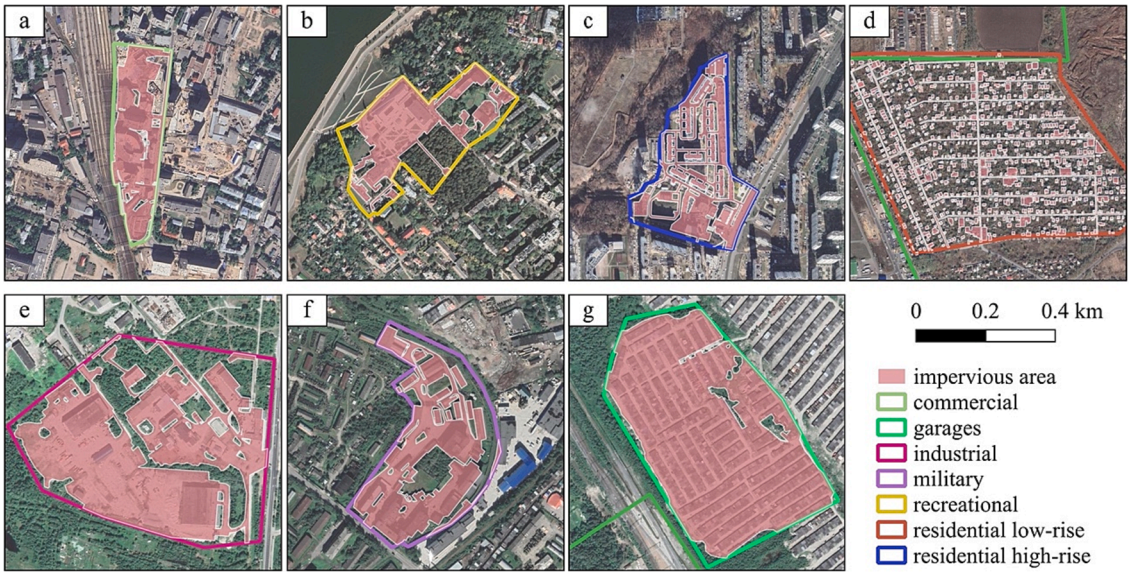

Fig. 4. Examples of test polygons with different land-use types defined in Moscow (a), Kaluga (b), Kursk (c), Rostov-on-Don (d), Apatity (e,g), and Murmansk (f). Basemap: Google Earth Image WMS.

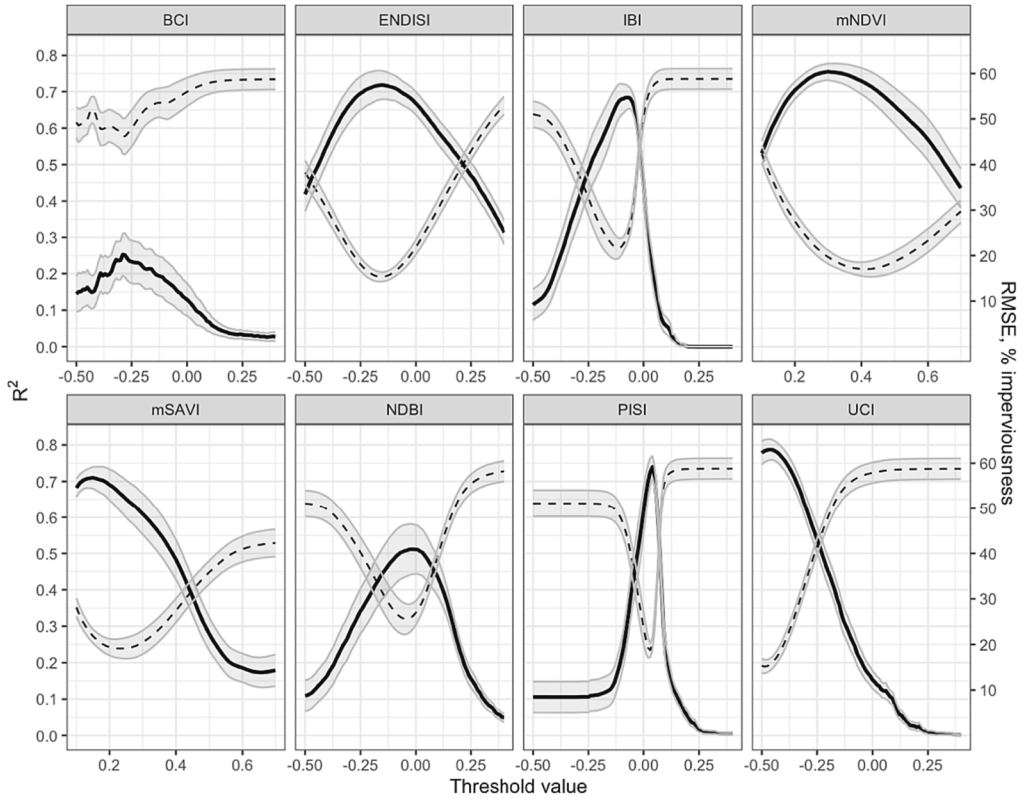

Fig. 5. The impact of threshold values on the performance metrics of different spectral indices on the impervious area percentage retreival (dashed line – RMSE metrics, ordinary line – R^2 metrics, grey fill = 95% confidence intervals) while compared with the validation dataset.

city; 5) added value of spectral mixture analysis. To our knowledge, there was no such a detail analysis of factors controlling the accuracy of impervious surface extraction from Sentinel-2 data.

Global land cover / impervious surface products are now also available, specifically by utilizing the Sentinel-1/Sentinel-2 data archives and other spatial data sources: European Space Agency (ESA) Worldcover (Zanaga et al., 2021), ESRI Land Cover at 10-m resolution (Karra et al., 2021), German Aerospace Agency (DLR) World Settlement Footprint 2019 (WSF2019) (Marconcini et al., 2021), global impervious surface area (GISA-10m) (Huang et al., 2022), and Hi-GISA (Sun et al., 2022). Global datasets could map impervious surface at a high accuracy (>70–80%) and are indeed a helpful tool for urban landscape parametrization. However, in urban studies and planning, annual dynamics of urban development are often required and the accuracy of 70% and less is practically insufficient for preparing a detailed masterplan. Moreover, due to spectral similarity of urban material and e.g. bare soils /

Table 2
Best metrics and thresholds across all indices (comlete dataset with all seasons obtained for individual cities).

Spectral index	Highest R^2	Lowest RMSE	Best threshold
BCI	0.252	46.171	−0.29
ENDISI	0.719	15.307	−0.15
IBI	0.684	21.628	−0.09
NDBI	0.512	25.589	−0.03
PISI	0.74	18.745	0.04
UCI	0.787	15.167	−0.47
mNDVI	0.755	16.977	0.35
mSAVI	0.71	19.119	0.19

croplands whose patches can often be found within the city boundaries, the total impervious area can be under- or overestimated leading to inaccuracies in the scientific inferences from the urban ecological studies. Therefore, the available global datasets require the validation at a local and regional scales.

2. Materials and methods

2.1. Test cities

We have chosen ten Russian cities different in climate, population, and type of economic activity. They are located across latitudes both in European Russia, Siberia, and Far East, covering the bioclimatic zones from subarctic to steppe (Fig. 1, Table 1).

2.2. Sentinel-2 data selection, processing, and approaches for mapping impervious surfaces

2.2.1. Satellite-based observation of phenology

For the territory of each city, we have selected images (or same date composites) taken within the onset (GSO), middle (GSM), and the end (GSE) of the growing season in the spring – autumn 2019 (if there were no suitable scenes, we have selected scenes taken in 2020). We have identified centers of these periods according to 16-day MODIS NDVI 250m (MOD13Q1) trend (Didan, 2021), and air temperature (at 2 m) trends according to Copernicus ERA5 reanalysis data (daily aggregates) (Muñoz Sabater, 2019). The onset and the end (middle date) of the growing season were defined as an average of two dates: 1) date of rapid increase/decline of MODIS NDVI values; 2) date of crossing the +5 °C surface temperature threshold. The GSO and GSE periods were defined as one week before and after the corresponding dates. The GSM has been determined as the plateau of the MODIS NDVI values. We have searched for Sentinel-2 images acquired within the defined GSO, GSM, and GSE periods. In addition, we have produced a median composite for each city covering the entire summer seasons of 2019 and 2020 (MC). The calculated periods and found Sentinel-2 acquisition dates are shown on Fig. 2.

2.2.2. Data pre-processing and assessment of algorithms for extraction impervious surfaces

We have used both L1C top-of-atmosphere (TOA) and L2A surface reflectance (SR) ESA Sentinel-2 data available within Google Earth Engine (Gorelick et al., 2017). TOA images were used to produce Tasseled Cap transformation values. SR data were all atmospherically corrected using *sen2cor* algorithm.

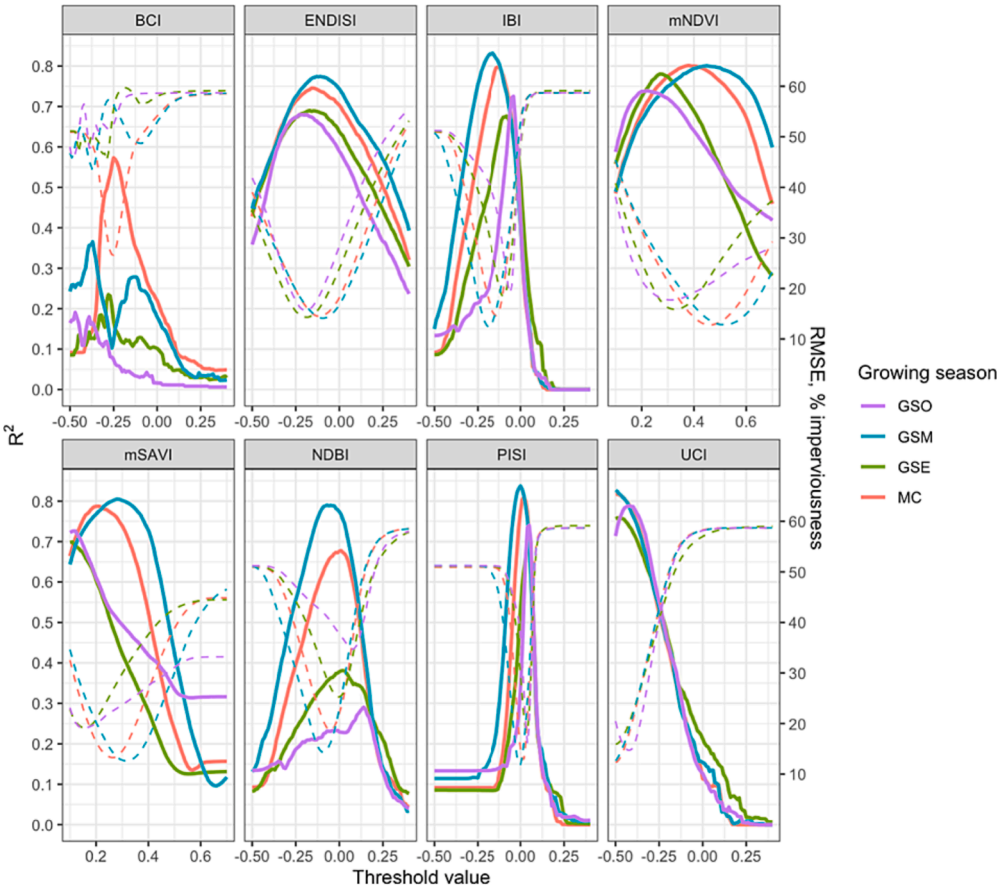

Fig. 6. The impact of threshold values on the performance metrics of different spectral indices on the impervious area percentage retreival depending on the growing season (dashed line – RMSE metrics, ordinary line – R^2 metrics) while compared with the validation dataset.

Table 3
Best RMSE and R^2 metrics for all cities depending on the growing season period (fr – indication of sub-pixel classifications). Best result is indicated as bold.

City	Month	Season	Index	Threshold	R^2	RMSE
Murmansk	June	GSO	mNDVI	0.45	0.74	10.24
	July	**GSM**	**mNDVI**	**0.48**	**0.85**	**7.87**
	October	GSE	mNDVI	0.28	0.68	12.21
	Median	MC	IBI	−0.17	0.75	11.06
Apatity	June	GSO	IBI	−0.2	0.97	5.34
	July	GSM	IBI	−0.22	0.96	5.34
	September	**GSE**	**ENDISI**	**−0.22**	**0.96**	**4.94**
	Median	MC	IBI	−0.21	0.96	5.37
Cherepovets	April	GSO	ENDISI	−0.22	0.76	12.88
	June	GSM	ENDISIfr	−0.18	0.82	12.89
	September	**GSE**	**NDBI**	**−0.03**	**0.83**	**11.02**
	Median	**MC**	**NDBI**	**−0.06**	**0.84**	**12.11**
Moscow	April	GSO	mNDVI	0.3	0.82	13.36
	June	GSM	mSAVI	0.34	0.76	14.88
	November	GSE	mSAVI	0.1	0.8	13.41
	Median	**MC**	**mSAVI**	**0.26**	**0.84**	**12.77**
Novosibirsk	May	GSO	mNDVI	0.4	0.89	7.87
	June	**GSM**	**IBIfr**	**−0.19**	**0.91**	**7.31**
	October	GSE	UCI	−0.49	0.89	8.07
	Median	MC	mNDVI	0.43	0.9	7.57
Pushchino	April	GSO	PISI	0.04	0.87	11.48
	June	GSM	PISI	−0.02	0.84	11.98
	October	GSE	mNDVI	0.39	0.89	10
	Median	**MC**	**NDBIfr**	**−0.06**	**0.89**	**9.84**
Kaluga	April	GSO	UCI	−0.39	0.86	9.3
	June	GSO	PISIfr	−0.02	0.81	10.79
	November	GSE	UCIfr	−0.47	0.84	9.59
	Median	**MC**	**PISI**	**0.01**	**0.87**	**9.02**
Kursk	April	GSO	UCI	−0.4	0.9	9.12
	June	**GSM**	**UCI**	**−0.5**	**0.94**	**7.68**
	November	GSE	mNDVI	0.26	0.93	7.75
	Median	**MC**	**PISI**	**0.03**	**0.94**	**7.76**
Rostov-on-Don	April	GSO	UCI	−0.5	0.89	7.64
	June	GSM	UCI	−0.5	0.89	7.39
	August	GSE	mNDVI	0.46	0.83	9.05
	October	GSE	mNDVI	0.35	0.89	7.52
	Median	**MC**	**UCI**	**−0.48**	**0.9**	**7.12**
Nakhodka	April	GSO	UCI	−0.41	0.64	10.84
	August	**GSM**	**NDBIfr**	**−0.12**	**0.91**	**5.19**
	November	GSE	IBI	−0.09	0.63	10.04
	Median	MC	IBI	−0.11	0.77	8.96

Several spectral transformation approaches were used to assess whether a pixel belonged to the "impervious surface" class. These transformations included per-pixel and sub-pixel classifications. We analyzed vegetation indices: modified NDVI (mNDVI) and modified SAVI (mSAVI). The modification is a rule-based approach described in (Dvornikov et al., 2021) that considers the Blue, NIR, SWIR1 and SWIR2 limits in addition to NDVI/SAVI thresholds (Fig. 3). The threshold here is the index value below which we consider the pixel as "impervious". For these two indices, we tested the sequence of thresholds from 0.1 to 0.7 with 0.01 step, 61 in total. Further, we have also tested a set of published built-up indices (NDBI (Zha et al., 2003), Improved Built-Up Index - IBI (Xu, 2008), BCI (Deng and Wu, 2012), Enhanced Normalized Difference Impervious Surface Index - ENDISI (Chen et al., 2019), Perpendicular Impervious Surface Index - PISI (Tian et al., 2018), and Urban Composition Index - UCI (Zhang et al., 2021) with threshold sequences from −0.5 to 0.4 with 0.01 step, 91 in total. While calculating BCI, we used Tasseled Cap transformation coefficients for ten (VIS-NIR-SWIR bands) from (Nedkov, 2017). Given the threshold step for each spectral index, we have obtained 668 estimates of impervious pixels in total. For each threshold value, a sub-pixel classification (fractions) was additionally produced using the created endmembers of seven LULC classes (~20 for each class): bare soil, dense forest, shrublands, grasslands, urban low albedo, urban high albedo (see e.g. Xu et al., 2018), and urban albedo color. Urban albedo color – buildings with colorful roofs (in Russian cities normally red, blue, and green colors can be found). Therefore, 1336 estimates were obtained for each image/composite, meaning that in total we have made 54,776 estimates for all cities/seasons. Prior to the analysis, we have applied water masks for all scenes extracted from the OpenStreetMap (OSM) vector data (*Key* = *'natural'*, *value* = *'water'*).

2.3. Validation and statistical processing

We have assessed the quality of our estimates on the aerial basis. Within each city, from 18 to 30 polygons were selected where detailed expert assessments (impervious area percentage) were made based on the very-high resolution Google Earth Image WMS Service. These polygons varied in area (from 0.75 to 162.91 ha, median – 11.4 ha) and represented seven different land-use types: recreational, residential low-rise houses, residential high-rise blockhouses, industrial, industrial-garages, military, and commercial (Fig. 4). These land-use classes were assigned both using the OSM data (*Key* = *'landuse'*) and by visual inspection (we have divided residential land-use type into low-rise and high-rise classes). The true impervious area percentage has been identified for each polygon (Fig. 4). Validation metrics (R^2, RMSE) were assessed for each estimate of imperviousness (mapped vs true). The relationships between metric and thresholds among seasons and pixel / sub-pixel approaches were statistically analyzed using the Kruskal-Wallis non-parametric test (Kruskal and Wallis, 1952). The impact of land-use type of the test areas was also assessed using a linear regression.

2.4. Comparison with global datasets

The best (according to metrics and visual inspection) impervious

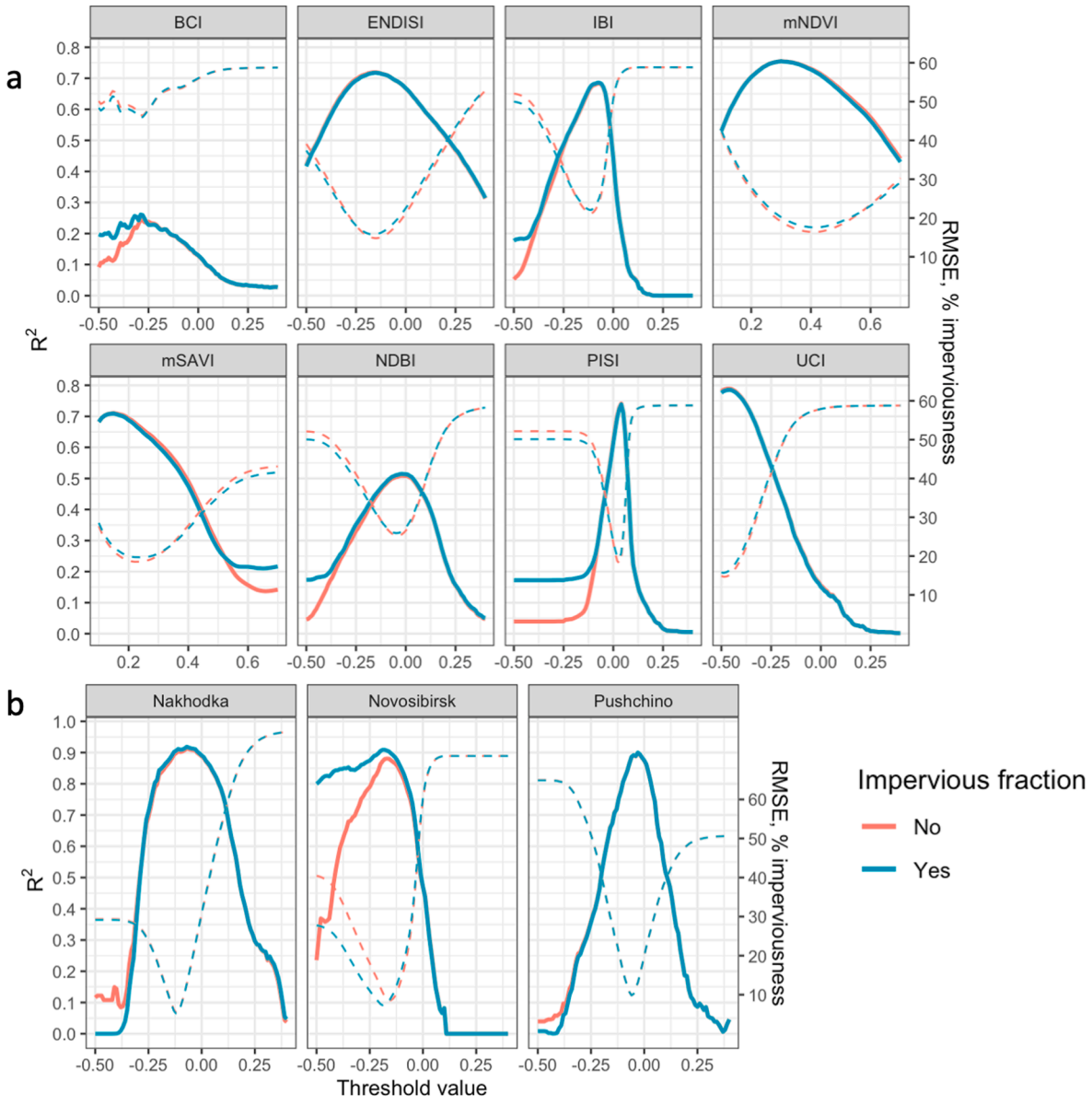

Fig. 7. a) Effect of sub-pixel classification of the extracted impervious pixels on the total R^2 (ordinary line) and RMSE (dashed line) metrics while compared with the validation dataset. b) Statistics for cities having best metrics with fractions: Nakhodka – NDBIfr (GSM), Novosibirsk – IBIfr (GSM), Pushchino – NDBIfr (MC) (Table 3), dashed line – RMSE metric, ordinary line – R^2 metric).

surface estimates were further compared with available global 10-m land cover/built-up datasets by calculating the same quality metrics. Four datasets were compared: 1) 10-m Sentinel-1/2-based ESA Worldcover (Zanaga et al., 2021); 2) Sentinel-2 based ESRI Land Cover (Karra et al., 2021); 3) 10-m Sentinel-1/2-based DLR WSF2019 (Marconcini et al., 2021) assessed through EOC Geoservice of the Earth Observation Center (EOC) website (https://download.geoservice.dlr.de/WSF2019/files/) and 4) global impervious surface area (GISA-10m) (Huang et al., 2022) assessed through the data portal (https://zenodo.org/record/5791855#.ZGIqsy9BxhE).

3. Results

3.1. Response of quality metrics depending on index/threshold (city-level)

IBI and PISI were threshold-sensitive across all cases, meaning that these indices might show a worse performance if unsuitable threshold value is chosen (Fig. 5). The best metrics were obtained with thresholds −0.09 for IBI and 0.04 for PISI. Small shifts in the PISI thresholds (below 0.02 and higher than 0.05) results in a rapid decline of R^2 and RMSE metrics. ENDISI, UCI and mNDVI indices have shown the best performance (Table 2). At thresholds −0.15, −0.47 and 0.35 they could reach the max R^2 of 0.73, 0.79 and 0.76 respectively. Herewith, four less threshold-sensitive spectral indices (mNDVI, mSAVI, ENDISI and UCI) could be considered as having a similar performance ($R^{2>}$0.7 and RMSE<20% on average). mNDVI and ENDISI have shown a stable results across a wide range of thresholds (0.2 – 0.45 for mNDVI and −0.25 – 0 for ENDISI).

Mean values of BCI thresholds have shown metrics below 0.3 for R^2 and above 40% for RMSE (Table 2). Moreover, the threshold-metric curve appeared to be unstable depending on the threshold value.

3.2. The impact of growing season on the mapping accuracy

Comparison of the GSO/GSE and GSM/MC has shown significantly better results for established growing season/median composite with all

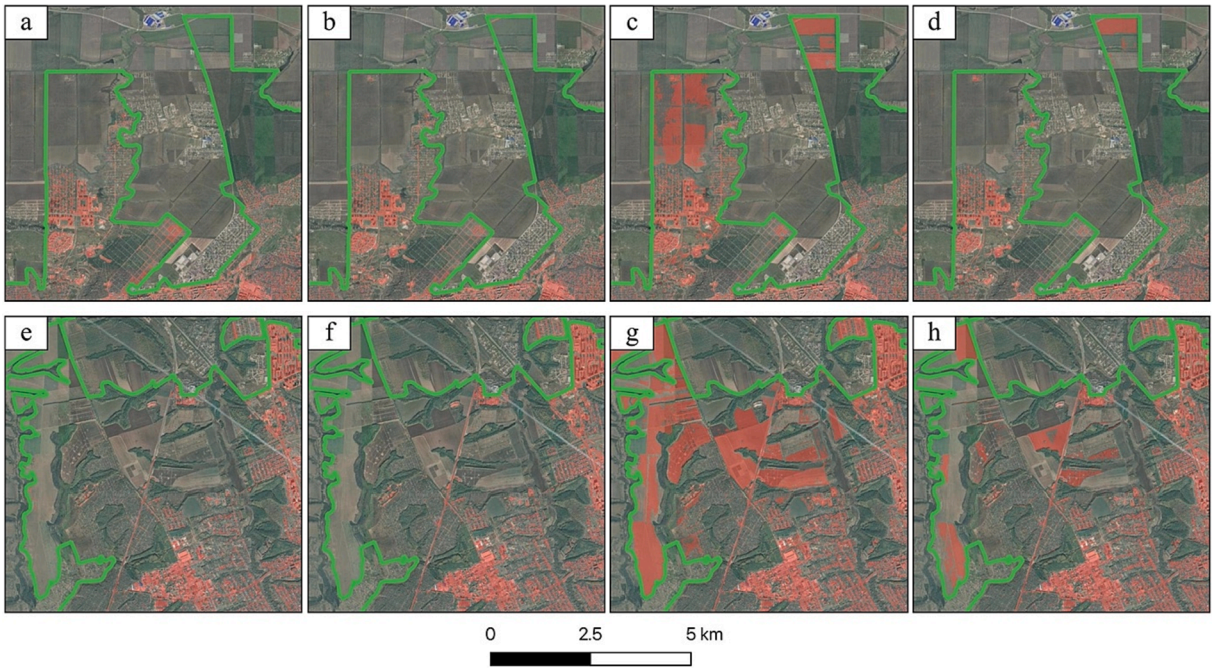

Fig. 8. Examples of impervious surface retrieval using the MC images for Rostov-on-Don (a-d) and Kursk (e-h): a,e – based on mNDVI, b,f -UCI, c,g – IBI, d,h – PISI. Green line – city boundary.

spectral indices except UCI and PISI where results for all seasons were comparable ($p>0.05$, *KW chi-squared* < 1, Fig. 6). Logically, modified vegetaion indices have demonstrated shifts in thresholds towards higher values from the beginning (0.22/0.12 for mNDVI/mSAVI) to the middle (0.45/0.28) of growing season and back to the end (0.27/0.11). GSM and MC had 3–5% lower RMSE for mNDVI, 6–7% lower RMSE for mSAVI, and generally less threshold-sensitive metrics (Fig. 6). Most of built-up indices (ENDISI, IBI, PISI and UCI) have shown a comparable metrics across seasons although GSM and MC were obviously better: mapped impervious area percentage with PISI, UCI and IBI thresholds explained 83% variance of real imperviousness, with ENDISI – 77%. That was 2–3% higher than in case of vegetation indices. Optimal thresholds for GSM and MC were 0.01, −0.49, −0.14 and −0.13 for PISI, UCI, IBI and ENDISI respectively. BCI has shown a non-robust results and lower metrics for all seasons, NDBI has shown acceptable results (R^2=0.79) for scenes taken within the GSM. Again, PISI and IBI were most threshold-sensitive indices for extracting the percentage of the impervious area.

When comparing the best metrics separately for all cities, there were no clear "best" season revelaed: in six cities (Cherepovets, Moscow, Pushchino, Kaluga, Kursk, Rostov-on-Don) the best metrics were obtained while using the two summer seasons MC. However, these metrics were also very close to other seasons (GSM or GSE in some cases) (Table 3). For Murmansk, Novosibirsk, Kursk and Nakhodka, the highest metrics were obtained for acquisitions taken during the established (GSM) growing season (Table 3). On average, the R^2 for all cases exceeded 0.85 (with maximal 0.97 for Apatity and minimal 0.63 for Nakhodka) while the mean RMSE was <9% (4.94% for Apatity – minimal value and 14.88% for Moscow – maximal value). All indices except BCI at least one time appeared in the final table of best metrics (Table 3), although the built-up indices were more frequent than vegetation ones.

3.3. Effect of additional spectral unmixing

When appliying the sub-pixel classification over the impervious area mask obtaining from spectral index thresholding (known as modified linear spectral mixture analysis, MLSMA), results still remain similar for both cases (with and without sub-pixel classification). The extraction of impervious fraction from the potentially impervious pixels didn't significantly improve final quality metrics (Fig. 7). Sometimes, assessments with impervious fractions have shown best metrics for scenes taken during the established growing season (GSM) characterized by „greenest" vegetation (Nakhodka, Novosibirsk, Table 3). Fractions have performed better only at the unapropriate threshold values (low for built-up indices – BCI, IBI, NDBI, PISI and high for vegetation index mSAVI). Statistically, fraction-datasets for all indices didn't significantly differ from non-fraction datasets ($p>0.05$, *KW chi-squared* < 1.8) except PISI index (Fig. 7).

3.4. Final maps and estimates of imperviousness compared to global datasets

The binary impervious area rasters based on indices and thresholds from the Table 3 (especially for GSE) had many affects within bare soils, agricultural fields, and urban forests land cover classes. Therefore, best performing indices with optimal thresholds obtained at the previous stages were further applied to GSM and MC images for all ten cities simultaneously: we have chosen mNDVI (0.41), IBI (-0.14), PISI (0.01), and UCI (-0.49). Above mentioned thresholds were chosen since they had the best metrics for the selected parts of growing season (Fig. 6). These eight estimates of imperviousness for each city were considered as final results. We have visually inspected these final rasters since optimal validation metrics obviously may not reflect the complete picture of correctly separated impervious pixels.

For all MC, UCI (-0.49) and mNDVI (0.41) correctly reflected the imperviousness within all cities. PISI could show the similar picture for several cities only (Novosibirsk, Pushchino, Kaluga, Nakhodka), IBI – for Cherepovets only. In other cities, PISI (0.01) and IBI (-0.14) had artefacts within bare soil and forest land cover classes (Fig. 8). For GSM period, UCI (-0.49) and mNDVI (0.41) were best for all cities except Moscow and Nakhodka. All four selected indices had close metrics when considering all test areas (n=254) in all cities (Fig. 9).

ESA Worldcover dataset (2020) and GISA-10m have shown a close performance compared to UCI and mNDVI (Fig. 10) whereas DLR WSF2019 underestimated and ESRI Land Cover significantly overestimated the impervious area percentages within the test areas in all ten

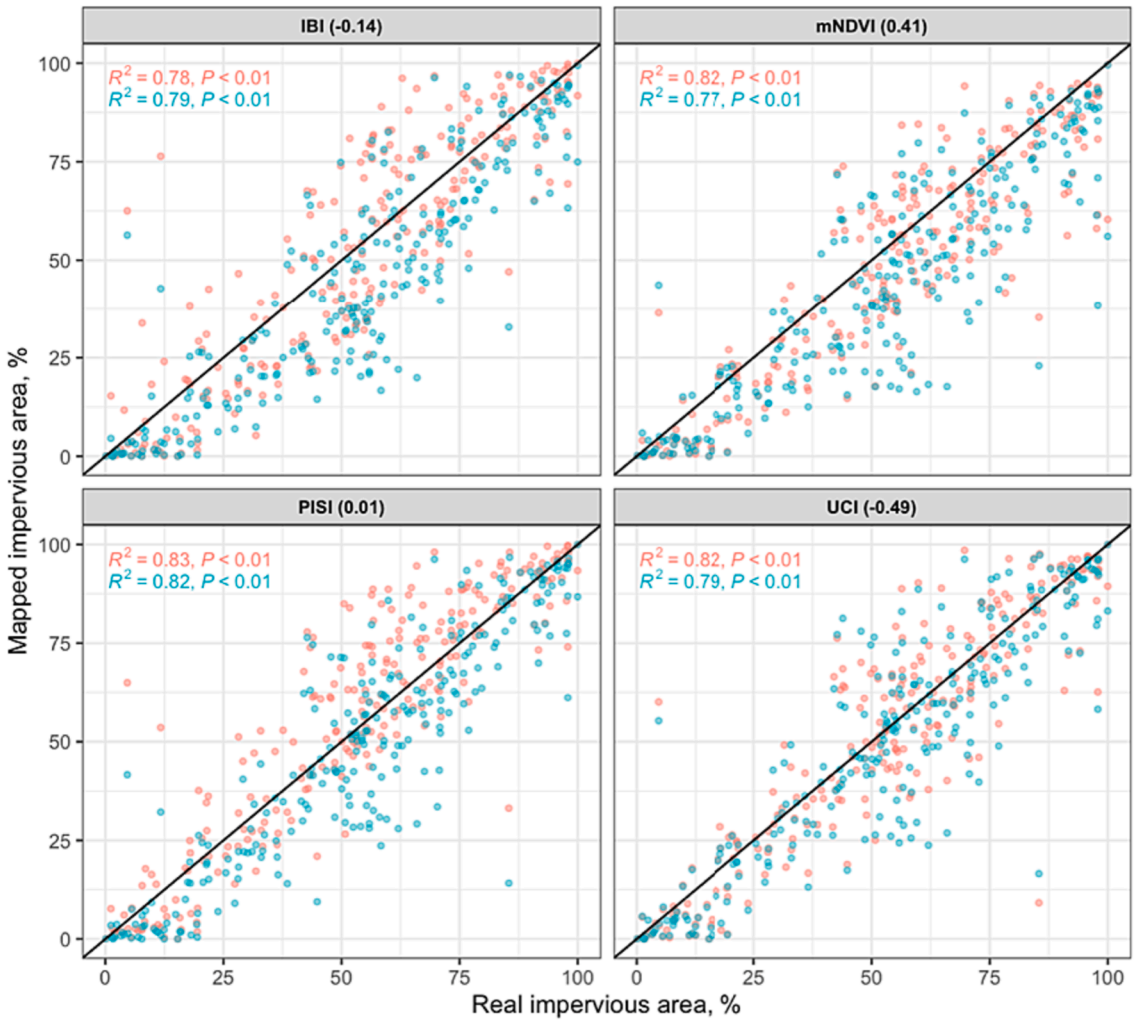

Fig. 9. Real and mapped percentage of impervious area for 254 test polygons in ten cities. Red dots – estimations based on 2019–2020 median composites (MC), blue dots – estimations based on GSM Sentinel-2 scenes.

cities (n=254). Overestimations of ESRI Land Cover are associated with within-urban landscapes uncertiainities – urban lawns and green infrastructure are mapped as impervious (Fig. 11). These overestimations contribute significantly in to the final imperviousness assessments of selected cities. On average, the WSF2019 underestimated the quasi-true imperviouseness by 22%, ESRI Land Cover – overestimated by 164%, and ESA Worlcover – overestimated by 3% only (Fig. 12). There were no difference between ESA and mNDVI/UCI estimates (*Wilcoxon rank sum test, p=0.73*). GISA-10m dataset tends to overestimate the real picture, but not significantly (Fig. 10).

Small-patchy urban structures (garages, residential low-rise houses) have obviously contributed more to the overall estimation error. When mapping with three best-performed indices (mNDVI, PISI, UCI) as well with the ESA Woldcover dataset, highest residuals while detecting imperviousness is expected within the garages (Fig. 13) – the residuals for this land-use type statistically differed from other land-use types in three cases except mNDVI (Fig. 13, $p < 0.05$, $16 < KW\ chi\text{-}squared < 23$). In case of PISI, residential low-rise, recreational, and military land-use types have also contributed significantly to the overall error. Linear regression with real imperviouseness (%) as target variable and mapped imperviouseness with land-use type as independent variables has shown that UCI approach is less sensitive to land-use type. For other approaches, garages, residential low-rise, and recreational land-use types can contribute to the fianl error ($p < 0.05$). mNDVI approach was less sensitive to outliers (Fig. 13).

4. Discussion

4.1. How do we define imperviousness?

The proportion of the urbanized area from the Earth's land area varies from 0.45 to 3% (Liu et al., 2014) depending on how to define it. Urban area may be defined as a composition of sealed moisture-impervious surfaces (roads, buildings, parking lots, etc.) or as built-up areas which are dominated by the built environment but still may include urban greenery or even urban administrative area with various surface properties.

Significant uncertainty in estimates of the urban area may be also caused by the spatial resolution of the satellite data. At first glance, the latter issue should become less relevant as new land cover datasets with 10-meter resolution become available. However, we show that even high-resolution datasets have significant differences in urban area estimates, so application of the global-oriented estimates for a city-scale urban parametrization is quite uncertain. This problem is related to discrepancy in urban area definition in different projects and datasets. The definitions used in the global datasets considered in our study are also not always consistent. GISA-10m is developed to map artificial impervious surfaces (Huang et al., 2022). WSF dataset is developed to map human settlements, where settlements are defined as areas coved by buildings, building lots, roads and paved-surfaces (Marconcini et al., 2020). ESA Worldcover dataset defines urban class as "land covered by

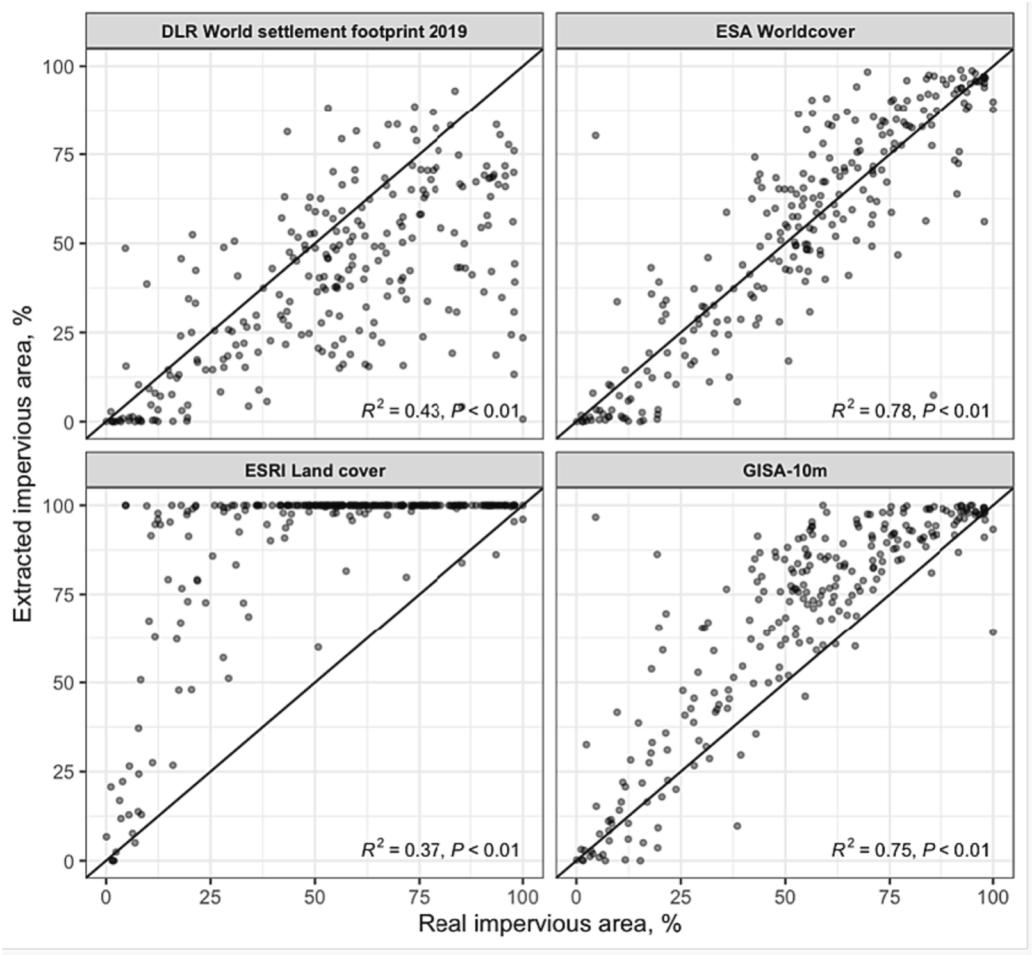

Fig. 10. Comparison of a true impervious area percentage with estimates made by different global datasets.

buildings, roads and other man-made structures", where urban greenery (parks, sport facilities) is not included in this class (Zanaga et al., 2021). Urban class definition in ESRI Land Cover is close to previous one ("Human made structures; major road and rail networks; large homogenous impervious surfaces including parking structures, office buildings and residential housing"), but without clarification about urban greenery (ESRI et al., 2022). Despite all definitions generally correspond to artificial impervious surfaces, our analysis demonstrated that the actual data not always represent surface imperviousness. ESRI Land Cover strongly overestimates the imperviousness; urban surfaces there include urban greenery and therefore better corresponds to building-dominated areas than to impervious areas. Less, but still significant overestimation of the reference imperviousness is typical for GISA-10m. WSF2019 data, on contrary, noticeably underestimates impervious, probably due additional restrictions applied according to settlement agreement mask at post-processing stage (Marconcini et al., 2020). Worldcover shows the best match to the reference data among the global datasets reviewed, but still lags behind the proposed approaches in terms of quality metrics. Revealed uncertainty of global datasets clearly illustrates the need for detailed datasets which can be obtained for individual cities following the proposed methods.

4.2. Imperviousness of Russian cities

Sun et al. (2022) estimated the global impervious area to be 1.29 Mio km^2 (2018) with Russia being a significant contributor (3rd place) to the total growth of the imperviousness from 2015 to 2018. Russian cities can often be characterized by vast areas built-up with low-rise residential houses, especially in the Russian South and in case of purposive inclusion of large suburban areas into official boundaries for artificial increase of city population. This may affect the accuracy of imperviousness assessment: e.g. ESA Worldcover dataset has shown to be significantly underestimating the built-up landcover class in *peri*-urban areas (Sun et al., 2022).

In general, there is practically no information about imperviousness in Russian cities verified by ground truth or very-high resolution images. Some scarce data exist for Moscow, Volgograd, Rostov-on-Don, and Murmansk, although in most cases the publications indicate the average impervious surface proportion for various land-use types (for example, residential, industrial, or recreational, etc.), which is far from the level of details needed for decision-making. A detailed mapping of impervious surfaces was carried out by the authors for Rostov-on-Don (27.6%, accuracy: R^2=0.84), Murmansk (17.5%, accuracy: R^2=0.81), and Moscow (21%) based on mSAVI index approach (threshold 0.28) to assess the impact of urbanization on the soil organic carbon stocks (Dvornikov et al., 2021; Vasenev et al., 2021). According to our current estimates (Fig. 12), Cherepovets with a considerable fraction of industrial areas had an imperviousness >30%, whereas the lowest value was shown for Pushchino – a town of science. Remaining eight cities were ~20% impervious on average. The proposed approaches will allow to define an accurate area of impervious surface in many other cities.

4.3. Overview of existing approaches for Sentinel-2 based mapping imperviousness

Increasing amount of satellite data and methods for its intellectual

Fig. 11. Mapped impervious surface for the area within Pushchino using different methods: a – mNDVI, b – UCI, c – ESA Worldcover, d – DLR WSF2019, e – ESRI Land cover, f – GISA-10m.

processing open a new horizon in change detection algorithms and modelling of urban sprawl / urban planning. Due to satisfactory spectral and spatial resolution for the extraction of imperviousness (Weng, 2012), Sentinel-2 data are capable in extracting even small urban and natural landscape structures (Radoux et al., 2016). The pixel-based spectral index approach is considered as a valuable tool for identification of impervious surfaces with an advantage of low processing time, simplicity, and the independent and easy calculation (Parekh et al., 2021). However, it requires the selection of the optimal threshold, which can be quite difficult (Lu et al., 2014). Here we present the optimal range of thresholds when applying different indices: several of them are less value sensitive (ENDISI, mNDVI, and mSAVI) than others (PISI, IBI, NDBI, UCI) (Figs. 5 and 6). Given the fast development of cloud-computing platforms (e.g. Google Earth Engine), the task of selecting of index thresholds can be solved by applying an iterative processing within a ranges presented here (see sub-section 2.2.2).

Among the published solutions for extracting high-accuracy impervious surface, two researches have reported the areal accuracy assessments and not pixel-based (Xian et al., 2019; Xu et al., 2018). Validated over three cities, these estimates have shown quality metrics similar to ours (R^2>0.77, Fig. 8). It seems that index-based segmentation remains most easy-to-implement and promising technique for extracting impervious surface. Indices (e.g. UCI, PISI, mNDVI) can also be used as an important predictors when applying machine learning algorithms.

Although it was reported, that combination of both index-threshold and LSMA approaches lead to better estimations of imperviousness (Fan et al., 2015; Li, 2020; Xian et al., 2019), our estimates for different bioclimatic conditions show that there are no added value to the overall accuracy of estimations while using MLSMA (if areal accuracy assessment is considered).

4.4. Impact of selected approaches and seasons

We have found that among considered indices, mNDVI (0.41) and UCI (-0.49) applied to MC are most suitable approaches for mapping impervious surfaces within urban landscapes as revealed from validation metrics and visual inspection of obtained binary classifications. PISI and IBI indices show a high accuracy extraction of imperviousness, but they had a greater number of affects mostly within agricultural fields and dense forests (Fig. 8). Still, PISI threshold 0.01 has shown a good picture of imperviousness without affects for several cities (Novosibirsk, Pushchino, Kaluga, Nakhodka), IBI (-0.14) – for Cherepovets. In the testing of different algorithms made by (Feng and Fan, 2021), PISI has demonstrated best performance among indices when mapping with Sentinel-2 at 10 and 20-m resolution.

Approach mNDVI implements an addition thresholds in Blue, NIR and SWIRs spectral bands that were also demonstrated to have an importance in extracting urban footprint while applying non-linear predictive models (tree bagging) since the artificial material having the strong reflectance in the Blue and SWIR ranges can confidently separate pixels from the agriculture or semi-natural features (Herold et al., 2003; Lefebvre et al., 2016).

Shadows within built-up areas and dense forests, agricultural fields, and urban blue infrastructure are naturally the main sources of errors when mapping imperviousness with optical data. These affects can partially be eliminated by using the summer season MC: our visual inspection of classified images has revealed that MC had less artefacts. Moreover, since the shadowed pixels can often be misclassified as water (Hodgson et al., 2003), here we have used the OSM water mask in order to handle potential shadowed areas and loss of imperviousness due to misclassified “impervious” pixels.

Our data clearly show the advantage of GSM and MC data over GSO and GSE when mapping imperviousness. Probably, it is linked to a more contrasting spectral response of artificial material compared to

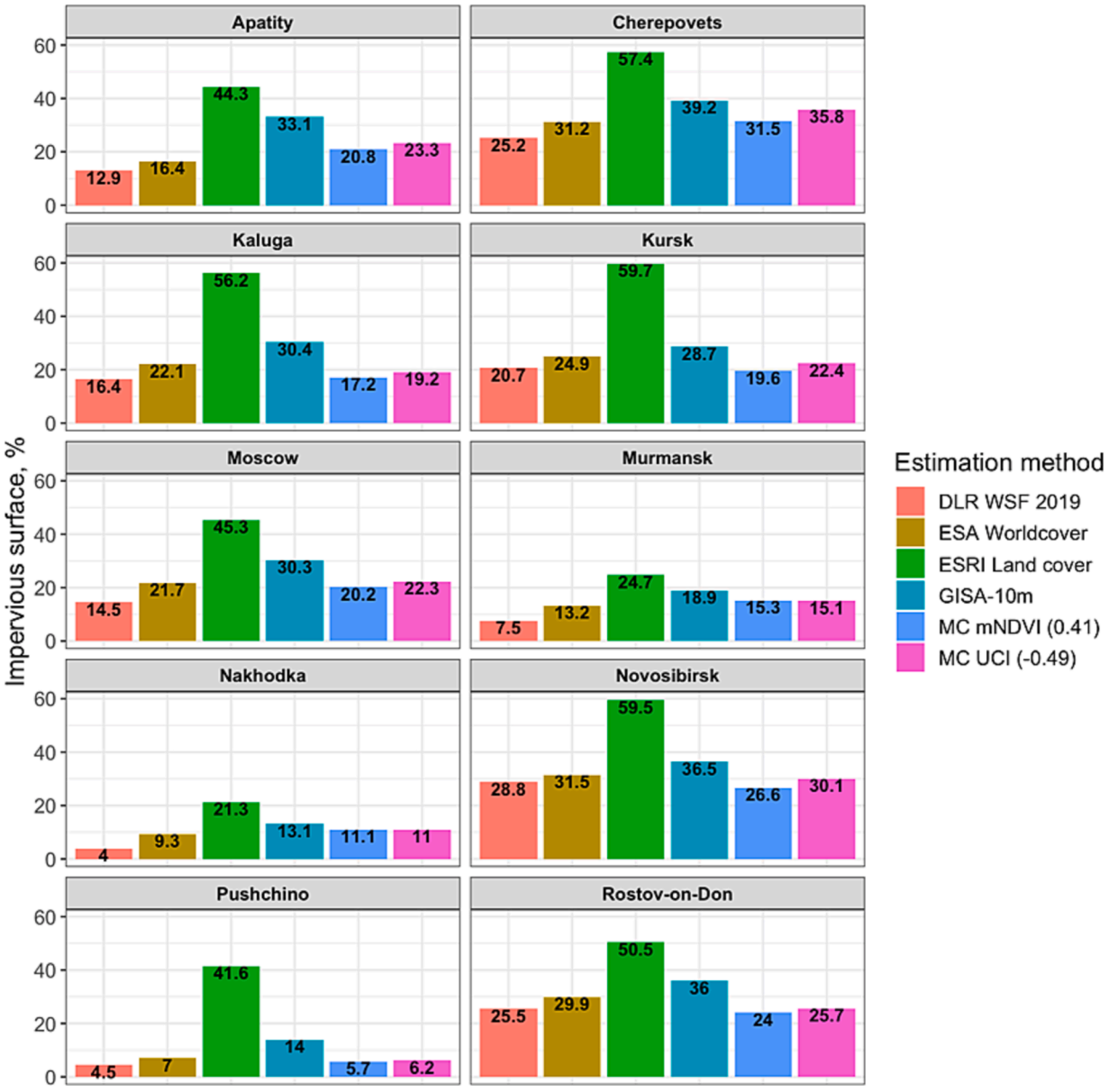

Fig. 12. Impervious area percentage assessments for ten cities made according to global datasets (WSF2019, GISA-10m, ESA and ESRI) as well as best performance approaches (mNDVI and UCI with MC).

vegetation / bare soils: when mapping imperviousness with images taken during the established growing season, there are less chances that bare soil pixels will be misclassified as impervious surface and vice-versa. Applying the ASTER image over the area of Indianapolis, it was found that summer acquisition was better in estimating imperviousness compared to a spring (April, GSO) and a fall (October, GSE) acquisitions (Weng, 2012).

5. Conclusions

Our main motivation of this research was to propose a set of recommendations for accurate mapping of impervious surface with Sentinel-2 data by conventional spectral transformation for the further use in urban ecological studies. Our results obtained for ten cities separately suggested that there is no best spectral index, as we hypothesized before carrying out this research: for different cities, the best metrics were obtained using all considered indices except BCI. Our statistical analysis simultaneously for all cities widely distributed in the geographic context reveals the obvious advantages of mNDVI (threshold 0.41) and UCI (threshold −0.49) indices, as they have shown best quality metrics and nearly no visually observed affects. The application of these indices/thresholds could provide an accurate estimate of imperviousness (with RMSE < 10%), better than given by any available global 10-m datasets (by minimum 5–10%).

It was clearly defined, that GSM and MC data have shown better impervious surface extraction, probably due to more contrasting spectral response compared with GSO and GSE data. For accurate imperviousness mapping, it is better to use the summer season median composites, since it can smooth shadows and enhance the signal from bare soils and agricultural fields. To extract imperviousness for the certain summer period, it is better to use acquisition taken during GSM.

The largest uncertainties are expected at areas with small-sized urban features (garages, low-rise houses). Our data also show, that an additional application of MLSMA over extracted impervious pixels doesn't lead to the improve of the mapping quality.

ESA Worldcover shows the best match to the reference data among the global datasets reviewed, but still lags behind the proposed approaches in terms of quality metrics. Moreover, compared global

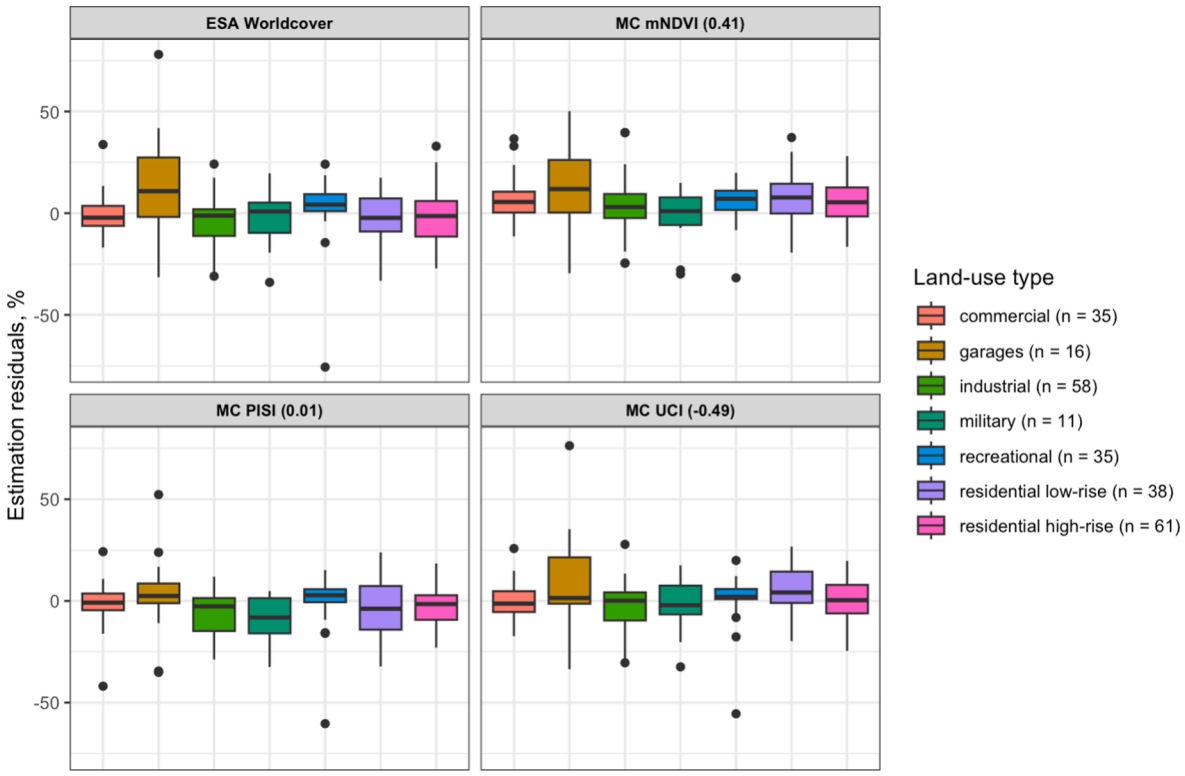

Fig. 13. Estimation residuals (delta between real and mapped) depending on the urban land-use type (n – number of test polygons belonging to the specific land-use type).

datasets demonstrate significant differences up to tens of percents between the impervious estimates for the selected cities, that highlights the relevance of our recommendations for detailed urban ecological studies. Revealed uncertainty of global datasets clearly illustrates the need for detailed products which can be obtained at the city-level scale following the proposed methods (indices/thresholds).

Funding sources

Remote sensing analysis and modelling were supported by the Russian Foundation Project N№19-77-300-12. Data processing and paper preparation were supported by the RUDN University Scientific Projects Grant System (N№202194-2-000), and governmental assignment N№122111000095-8.

CRediT authorship contribution statement

Yury Dvornikov: Conceptualization, Methodology, Software, Validation, Data curation, Writing – original draft, Writing – review & editing, Funding acquisition, Supervision. **Valentina Grigorieva:** Software, Validation, Writing – review & editing. **Mikhail Varentsov:** Conceptualization, Software, Data curation, Writing – original draft, Writing – review & editing. **Viacheslav Vasenev:** Conceptualization, Writing – review & editing, Funding acquisition, Supervision.

Declaration of Competing Interest

The authors declare that they have no known competing financial interests or personal relationships that could have appeared to influence the work reported in this paper.

Data availability

The main processing code and geospatial data are available at https://github.com/ydvornikov/Sentinel2_impervious_optimal.git.

Acknowledgement

We thank student assistants Veronika Krapivina, Daria Ivanova, and Anastasia Matina for preparing the validation dataset.

References

Anderson, J.R., Hardy, E.E., Roach, J.T., Witmer, R.E., 1976. A Land Use And Land Cover Classification System For Use With Remote Sensor Data.

Apreda, C., Schulz, J.-P., Reder, A., Mercogliano, P., 2023. Survey of land cover datasets for updating the imperviousness field in urban parameterisation scheme TERRA_URB for climate and weather applications. Urban Clim. 49, 101535 https://doi.org/10.1016/j.uclim.2023.101535.

Arnold, C.L., Gibbons, C.J., 1996. Impervious Surface Coverage: The Emergence of a Key Environmental Indicator. J. Am. Plan. Assoc. 62, 243–258.

Beck, H.E., Zimmermann, N.E., McVicar, T.R., Vergopolan, N., Berg, A., Wood, E.F., 2018. Present and future Köppen-Geiger climate classification maps at 1-km resolution. Sci. Data 5, 180214. https://doi.org/10.1038/sdata.2018.214.

Ceccarelli, T., Bajocco, S., Perini, L.L., Salvati, L., 2014. Urbanisation and land take of high quality agricultural soils - Exploring long-term land use changes and land capability in Northern Italy. Int. J. Environ. Res. 1, 181–192. 10.22059/IJER.2014.707.

Chen, J., Yang, K., Chen, S., Yang, C., Zhang, S., He, L., 2019. Enhanced normalized difference index for impervious surface area estimation at the plateau basin scale. J. Appl. Remote Sens. 13, 016502 https://doi.org/10.1117/1.jrs.13.016502.

Deng, C., Wu, C., 2012. BCI: A biophysical composition index for remote sensing of urban environments. Remote Sens. Environ. 127, 247–259. https://doi.org/10.1016/j.rse.2012.09.009.

Didan, K., 2021. MODIS/Terra Vegetation Indices 16-Day L3 Global 250m SIN Grid V061 [Data set] [WWW Document]. NASA EOSDIS L. Process. DAAC. 10.5067/MODIS/MOD13Q1.061.

Dvornikov, Y.A., Vasenev, V.I., Romzaykina, O.N., Grigorieva, V.E., Litvinov, Y.A., Gorbov, S.N., Dolgikh, A.V., Korneykova, M.V., Gosse, D.D., 2021. Projecting the urbanization effect on soil organic carbon stocks in polar and steppe areas of European Russia by remote sensing. Geoderma 399, 115039. https://doi.org/10.1016/j.geoderma.2021.115039.

EEA, 2010. The European environment – State and Outlook 2010: Soil. Copenhagen.

Ehlers, M., Jadkowski, M.A., Howard, R.R., Brostuen, D.E., 1990. Application of SPOT data for regional growth analysis and local planning. Photogramm. Eng. Remote Sens. 56, 175–180.

ESRI, ImpactObservatory, Microsoft, 2022. Sentinel-2 10m land use/land cover time series of the world [WWW Document]. URL https://www.arcgis.com/home/item.html?id=cfcb7609de5f478eb7666240902d4d3d.
European Commission, 2012. Guidelines on best practice to limit, mitigate or compensate soil sealing. Luxembourg. https://doi.org/10.2779/75498.
Fan, F., Fan, W., Weng, Q., 2015. Improving Urban Impervious Surface Mapping by Linear Spectral Mixture Analysis and Using Spectral Indices. Can. J. Remote. Sens. 41, 577–586. https://doi.org/10.1080/07038992.2015.1112730.
Feng, S., Fan, F., 2021. Impervious surface extraction based on different methods from multiple spatial resolution images: a comprehensive comparison. Int. J. Digit. Earth 14, 1148–1174. https://doi.org/10.1080/17538947.2021.1936227.
Gong, P., Howarth, P.J., 1990. The use of structural information for improving land-cover classification accuracies at the rural-urban fringe. Photogramm. Eng. Remote Sens. 56, 67–73.
Gorelick, N., Hancher, M., Dixon, M., Ilyushchenko, S., Thau, D., Moore, R., 2017. Google Earth Engine: Planetary-scale geospatial analysis for everyone. Remote Sens. Environ. 202, 18–27. https://doi.org/10.1016/J.RSE.2017.06.031.
Herold, M., Liu, X.H., Clarke, K.C., 2003. Spatial metrics and image texture for mapping urban land use. Photogramm. Eng. Remote Sensing 69, 991–1001. 10.14358/PERS.69.9.991.
Hodgson, M.E., Jensen, J.R., Tullis, J.A., Riordan, K.D., Archer, C.M., 2003. Synergistic use of lidar and color aerial photography for mapping urban parcel imperviousness. Photogramm. Eng. Remote Sensing 69, 973–980. 10.14358/PERS.69.9.973.
Huang, X., Yang, J., Wang, W., Liu, Z., 2022. Mapping 10 m global impervious surface area (GISA-10m) using multi-source geospatial data. Earth Syst. Sci. Data 14, 3649–3672. https://doi.org/10.5194/essd-14-3649-2022.
Jackson, T.J., McCuen, R.H., 1979. Accuracy of Impervious Area Values Estimated Using Remotely Sensed Data. J. Am. Water Resour. Assoc. 15, 436–446. https://doi.org/10.1111/j.1752-1688.1979.tb00346.x.
Jackson, T.J., 1975. Computer Aided Techniques for Estimating the Percent of Impervious Area from Landsat Data, in: Proceedings of the Workshop on Environmental Applications of Multispectral Imagery. American Society of Photogrammetry, Fort Belvoir, Virginia.
Kabisch, N., Haase, D., 2013. Green spaces of European cities revisited for 1990–2006. Landsc. Urban Plan. 110, 113–122. https://doi.org/10.1016/j.landurbplan.2012.10.017.
Karger, D.N., Conrad, O., Böhner, J., Kawohl, T., Kreft, H., Soria-Auza, R.W., Zimmermann, N.E., Linder, P., Kessler, M., 2017. Climatologies at high resolution for the Earth land surface areas. Sci. Data 4, 170122. 10.1038/sdata.2017.122.
Karra, K., Kontgis, C., Statman-Weil, Z., Mazzariello, J.C., Mathis, M., Brumby, S.P., 2021. Global Land Use/Land Cover With Sentinel 2 and Deep Learning. Int. Geosci. Remote Sens. Symp. 4704–4707 https://doi.org/10.1109/IGARSS47720.2021.9553499.
Kruskal, W.H., Wallis, W.A., 1952. Use of Ranks in One-Criterion Variance Analysis. J. Am. Stat. Assoc. 47, 583–621.
Lefebvre, A., Sannier, C., Corpetti, T., 2016. Monitoring urban areas with Sentinel-2A data: Application to the update of the Copernicus High Resolution Layer Imperviousness Degree. Remote Sens. 8, 606. https://doi.org/10.3390/rs8070606.
Li, W., 2020. Mapping urban impervious surfaces by using spectral mixture analysis and spectral indices. Remote Sens. 12, 94. https://doi.org/10.3390/RS12010094.
Liu, Z., He, C., Zhou, Y., Wu, J., 2014. How much of the world's land has been urbanized, really? A hierarchical framework for avoiding confusion. Landsc. Ecol. 29, 763–771. https://doi.org/10.1007/s10980-014-0034-y.
Lu, D., Li, G., Kuang, W., Moran, E., 2014. Methods to extract impervious surface areas from satellite images. Int. J. Digit. Earth 7, 93–112. https://doi.org/10.1080/17538947.2013.866173.
Marconcini, M., Metz-Marconcini, A., Üreyen, S., Palacios-Lopez, D., Hanke, W., Bachofer, F., Zeidler, J., Esch, T., Gorelick, N., Kakarla, A., Paganini, M., Strano, E., 2020. Outlining where humans live, the World Settlement Footprint 2015. Sci. Data 7, 242. https://doi.org/10.1038/s41597-020-00580-5.
Marconcini, M., Metz-Marconcini, A., Esch, T., Gorelick, N., 2021. Understanding current trends in global urbanisation - The world settlement footprint suite. GI_Forum 9, 33–38. https://doi.org/10.1553/GISCIENCE2021_01_S33.
Masson, V., Heldens, W., Bocher, E., Bonhomme, M., Bucher, B., Burmeister, C., de Munck, C., Esch, T., Hidalgo, J., Kanani-Sühring, F., Kwok, Y.-T., Lemonsu, A., Lévy, J.-P., Maronga, B., Pavlik, D., Petit, G., See, L., Schoetter, R., Tornay, N., Votsis, A., Zeidler, J., 2020. City-descriptive input data for urban climate models: Model requirements, data sources and challenges. Urban Clim. 31, 100536 https://doi.org/10.1016/j.uclim.2019.100536.
Morgan, K.M., Newland, L.W., Weber, E., Busbey, A.B., 1993. Using SPOT satellite data to map impervious cover for urban runoff predictions. Toxicol. Environ. Chem. 40, 11–16. https://doi.org/10.1080/02772249309357927.
Muñoz Sabater, J., 2019. ERA5-Land monthly averaged data from 1981 to present [WWW Document]. Copernicus Clim. Chang. Serv. Clim. Data Store. doi: 10.24381/cds.68d2bb30.
Nedkov, R., 2017. Orthogonal transformation of segmented images from the satellite Sentinel-2. Comptes Rendus L'Academie Bulg. des Sci. 70, 687–692.
Parekh, J.R., Poortinga, A., Bhandari, B., Mayer, T., Saah, D., Chishtie, F., 2021. Automatic Detection of Impervious Surfaces from Remotely Sensed Data Using Deep Learning. Remote Sens. 13, 3166. https://doi.org/10.3390/rs13163166.
Piotrowska-Długosz, A., Charzyński, P., 2015. The impact of the soil sealing degree on microbial biomass, enzymatic activity, and physicochemical properties in the Ekranic Technosols of Toruń (Poland). J. Soil. Sediment. 15, 47–59. https://doi.org/10.1007/s11368-014-0963-8.
Plunk, D.E., Morgan, K., Newland, L., 1990. Mapping impervious cover using Landstat TM data. J. Soil Water Conserv. 45, 589–591.
Radoux, J., Chomé, G., Jacques, D., Waldner, F., Bellemans, N., Matton, N., Lamarche, C., D'Andrimont, R., Defourny, P., 2016. Sentinel-2's Potential for Sub-Pixel Landscape Feature Detection. Remote Sens. 8, 488. https://doi.org/10.3390/rs8060488.
Romzaykina, O.N., Vasenev, V.I., Andrianova, D., Neaman, A., Gosse, D.D., 2020. The Effect of Sealing on Soil Carbon Stocks in New Moscow. In: Vasenev, V., Dovletyarova, E., Cheng, Z., Valentini, R., Calfapietra, C. (Eds.), Green Technologies and Infrastructure to Enhance Urban Ecosystem Services. SSC-2018. Springer, Cham, pp. 29–36. https://doi.org/10.1007/978-3-030-16091-3_5.
Romzaykina, O.N., Vasenev, V.I., Paltseva, A., Kuzyakov, Y.V., Neaman, A., Dovletyarova, E.A., 2021. Assessing and mapping urban soils as geochemical barriers for contamination by heavy metal(loid)s in Moscow megapolis. J. Environ. Qual. 50, 22–37. https://doi.org/10.1002/jeq2.20142.
Slonecker, E.T., Jennings, D.B., Garofalo, D., 2001. Remote sensing of impervious surfaces: A review. Remote Sens. Rev. 20, 227–255. https://doi.org/10.1080/02757250109532436.
Sun, Z., Du, W., Jiang, H., Weng, Q., Guo, H., Han, Y., Xing, Q., Ma, Y., 2022. Global 10-m impervious surface area mapping: A big earth data based extraction and updating approach. Int. J. Appl. Earth Obs. Geoinf. 109, 102800 https://doi.org/10.1016/j.jag.2022.102800.
Tian, Y., Chen, H., Song, Q., Zheng, K., 2018. A novel index for impervious surface area mapping: Development and validation. Remote Sens. 10 https://doi.org/10.3390/rs10101521.
Tucker, C.J., 1979. Red and photographic infrared linear combinations for monitoring vegetation. Remote Sens. Environ. 8, 127–150. https://doi.org/10.1016/0034-4257(79)90013-0.
Varentsov, M.I., Samsonov, T.E., Demuzere, M., 2020. Impact of Urban Canopy Parameters on a Megacity's Modelled Thermal Environment. Atmosphere (Basel). 11, 1349. https://doi.org/10.3390/atmos11121349.
Vasenev, V.I., Varentsov, M.I., Konstantinov, P.I., Romzaykina, O.N., Kanareykina, I., Dvornikov, Y.A., Manukyan, V., 2021. Projecting urban heat island effect on the spatial-temporal variation of microbial respiration in urban soils of Moscow megalopolis. Sci. Total Environ. 786, 147457 https://doi.org/10.1016/j.scitotenv.2021.147457.
Welch, R., 1982. Spatial resolution requirements for urban studies. Int. J. Remote Sens. 3, 139–146. https://doi.org/10.1080/01431168208948387.
Weng, Q., 2012. Remote sensing of impervious surfaces in the urban areas: requirements, methods, and trends. Remote Sens. Environ. 117, 34–49. https://doi.org/10.1016/j.rse.2011.02.030.
Xian, G., Shi, H., Dewitz, J., Wu, Z., 2019. Performances of WorldView-3, Sentinel-2, and Landsat-8 data in mapping impervious surface. Remote Sens. Appl.: Soc. Environ. 100246 https://doi.org/10.1016/j.rsase.2019.100246.
Xiao, R., Su, S., Zhang, Z., Qi, J., Jiang, D., Wu, J., 2013. Dynamics of soil sealing and soil landscape patterns under rapid urbanization. Catena 109, 1–12. https://doi.org/10.1016/j.catena.2013.05.004.
Xu, H., 2008. A new index for delineating built-up land features in satellite imagery. Int. J. Remote Sens. 29, 4269–4276. https://doi.org/10.1080/01431160802039957.
Xu, R., Liu, J., Xu, J., 2018. Extraction of high-precision urban impervious surfaces from Sentinel-2 multispectral imagery via modified Linear Spectral Mixture Analysis. Sensors 2873. https://doi.org/10.3390/s18092873.
Zanaga, D., Van De Kerchove, R., De Keersmaecker, W., Souverijns, N., Brockmann, C., Quast, R., Wevers, J., Grosu, A., Paccini, A., Vergnaud, S., Cartus, O., Santoro, M., Fritz, S., Georgieva, I., Lesiv, M., Carter, S., Herold, M., Li, L., Tsendbazar, N.E., Ramoino, F., Arino, O., 2021. ESA WorldCover 10 m 2020 v100. 10.5281/zenodo.5571936.
Zha, Y., Gao, J., Ni, S., 2003. Use of normalized difference built-up index in automatically mapping urban areas from TM imagery. Int. J. Remote Sens. 24, 583–594. https://doi.org/10.1080/01431160304987.
Zhang, L., Tian, Y., Liu, Q., 2021. A novel urban composition index based on water-impervious surface-pervious surface (W-I-P) model for urban compositions mapping using Landsat imagery. Remote Sens. 13, 3. https://doi.org/10.3390/rs13010003.
Zhang, Y., Zhang, H., Lin, H., 2014. Improving the impervious surface estimation with combined use of optical and SAR remote sensing images. Remote Sens. Environ. 141, 155–167. https://doi.org/10.1016/j.rse.2013.10.028.